Journal of Applied Polymer Science

A New Method to Prepare Low Melting Point Polyamide-6 and Study Crystallization Behavior of Polyamide-6/Calcium Chloride Complex by Rheological Method

Dianxin Liu,[1,2] Qiang Zheng,[1] Shengjun Lu,[1,2] Cheng Li,[1,2] Pan Lu,[1,2] Jie Yu[2]

[1]College of Materials and Metallurgy, Guizhou University, Guiyang 550025, Guizhou, China

[2]National Engineering Research Center for Compounding and Modification of Polymeric Materials, Guiyang 550014, Guizhou, China

Correspondence to: S. Lu (E-mail: mm.sjlv@gzu.edu.cn) and J. Yu (E-mail: yujiegz@126.com)

ABSTRACT: A new method to prepare low melting point polyamide-6 (LPA6) by complex reaction of calcium chloride ($CaCl_2$) and polyamide-6 (PA6) in a co-rotating twin screw extruder was reported. We employed a new rheological method to study the crystallization behavior of PA6/$CaCl_2$ complex and the mechanism of confined crystallization of PA6. Compared with differential scanning calorimetry (DSC), this method was more capable of detecting crystalline information. What's more, it was also an effective method for studying mechanism of confined crystallization. From the results of X-ray diffraction, DSC, infrared spectroscopy, rheology, and mechanical properties, the complex reaction of $CaCl_2$ with the carbonyl oxygen atom in the amide group disrupted the intermolecular hydrogen bonding and confined the mobility of PA6 molecules. This could significantly reduce the crystallinity and melting temperature of PA6, and improve tensile strength and notched Izod impact strength. © 2014 Wiley Periodicals, Inc. J. Appl. Polym. Sci. **2015**, *132*, 41513.

KEYWORDS: crystallization; differential scanning calorimetry (DSC); polyamides; rheology

Received 28 April 2014; accepted 12 September 2014
DOI: 10.1002/app.41513

INTRODUCTION

Polyamide-6 (PA6) as one of the most important thermoplastic accounts for a majority of the engineering products such as electronic equipments, automotive parts, and packaging materials because of its excellent stiffness, strength, thermal stability, and chemical resistance.[1,2] Besides, PA6 is usually used as a modifier to improve strength and toughness of other polymers.[3,4] However, PA6 is difficult to blend with other polymers in low processing temperatures, because PA6 has high melting point at high crystallinity. So it is significant to develop low melting point PA6 (LPA6).

DuPont and other institution have prepared LPA6 by restricting crystallization of PA, which is mostly prepared by the copolymerization method.[5–7] Because the synthesis process of this method is intricate and time-consuming, the application of LPA6 is limited. Several attempts have been made to prepare LPA6 for blending with the polymers of low processing temperatures. Xiong et al. prepared super-fine PA6 powders with a melting point of 189°C via jet-milling.[8] Afshari et al. reduced the crystallinity and size of crystalline grain of PA6 by complexation between gallium chloride ($GaCl_3$) and PA6.[9] Dong et al. prepared a styrene-maleic anhydride (SMA)-*g*-PA6 with a melting point of 187°C via solution graft reaction between SMA and PA6.[10]

Some scholars believed that the lewis acids such as lithium chloride (LiCl) and $GaCl_3$ can react with the amide group in PA6 and disrupt crystal structures,[11,12] which opens up a new way to exploit LPA6. Recently, our group found a neoteric melting extrusion way to continuously prepare LPA6 with a melting point of 198°C by melting complex reaction between PA6 and calcium chloride ($CaCl_2$).[13] However, as far as we know, no investigation has ever been reported regarding the mechanism of confined crystallization of PA6. It is well known that crystal structure change is extremely important to exploit LPA6. What's more, some scholars[14,15] studied crystallization behavior of PA6 only by differential scanning calorimetry (DSC) and X-ray diffraction (XRD) characterization methods. Because the DSC cannot record process of nucleation and growth of confined crystallization of PA6 seriously with considerably small heat flux, the real crystallization behavior of PA6 could not be detected. Crystal structure change of polymer would cause change of the modulus and viscosity, and rheology can be sensitive to reflect the movement of molecular chain. This study

focuses on the effects of the crystallization behavior of PA6/$CaCl_2$ complex and the mechanism of confined crystallization of PA6 with different contents of $CaCl_2$.

EXPERIMENTAL

Materials

PA6 (1013b) was obtained from UBE Co. Ltd., Japan. Calcium chloride ($CaCl_2$) (AR) was obtained from Chengdu Linjiang Chemical Co. Ltd., China.

Sample Preparation

$CaCl_2$ pellets were grinded using a high mixing machine for 40 min, and then sieved with 150 microns to obtain fine powders. PA6 pellets and $CaCl_2$ powders were dried in a vacuum oven at 80°C for 12 h. After blending $CaCl_2$ powders in PA6 pellets, the PA6/$CaCl_2$ samples were supplanted by twin-screw extruder (TSE-40A, Nanjing Ruiya polymer processing equipment Co., China). Temperature range from feeding to die was 200, 205, 210, 215, 220, 225, 230, 235, 240, and 240°C, and the screw rotation speed was l60 rpm. The PA6/$CaCl_2$ samples obtained from extruder were cut into the pellet at room temperature and dried in a vacuum oven at 80°C for 12 h. The PA6/$CaCl_2$ samples for XRD and mechanical properties were prepared by injection molding machine (CJ80m3V, Zhengde, China). Temperature range from feeding to die was 210, 220, 230, 235, and 240°C. The PA6/$CaCl_2$ samples obtained from injection molding were cut into blocks (5 mg) for DSC measurement. Besides, the PA6/$CaCl_2$ samples for rheological tests were prepared by compression molding (XLB-D350, Qingdao Xueqing equipment Co., China) at 230°C under 10 MPa to prepare disks of 1.5 mm in thickness and 25 mm in diameter.

Characterization

Rheology. Rheological measurements were performed on advanced rheometric expansion system (ARES, TA Instrument, USA) using parallel plate mode. All tests were kept about 1.0 mm gap distance. The frequency sweeps at 230°C were performed in the frequency range of 0.1–600 rad/s in the linearity region. Temperature sweeps from 230°C to 80°C were conducted at a constant cooling rate of 10 °C/min at strain amplitude of 0.5%.

Fourier Transform Infrared Spectroscopy. Fourier transform infrared spectroscopy (FTIR) was performed on potassium bromide (KBr) pellets using spectrometer (NEXUS670, Thermo Instrument, USA). The powders of the samples mixed with KBr were compressed into plates for FTIR analysis. The samples were analyzed in the spectral range of 400–4000 cm^{-1} at room temperature. The spectral resolution was 4 cm^{-1}.

Differential Scanning Calorimetry. Thermal properties were determined by DSC (PEDSC-2C, Thermo Instrument, USA) under purging gas (40 mL/min). The samples were quickly heated to 250°C and kept for 10 min to eliminate the thermal history, and then measurements between 40°C and 250°C were carried out at a constant cooling or heating rate of 10 °C/min. The thermograms were recorded for the calculation of thermal properties.

X-ray Diffraction. XRD was measured on a wide angle goniometer (D/MAX-2200, Rigaku X-ray diffraction, Japan) using Cu K_α radiation at 40 kV and 30 mA. All samples were scanned from 10° to 40° with a speed of 2°/min.

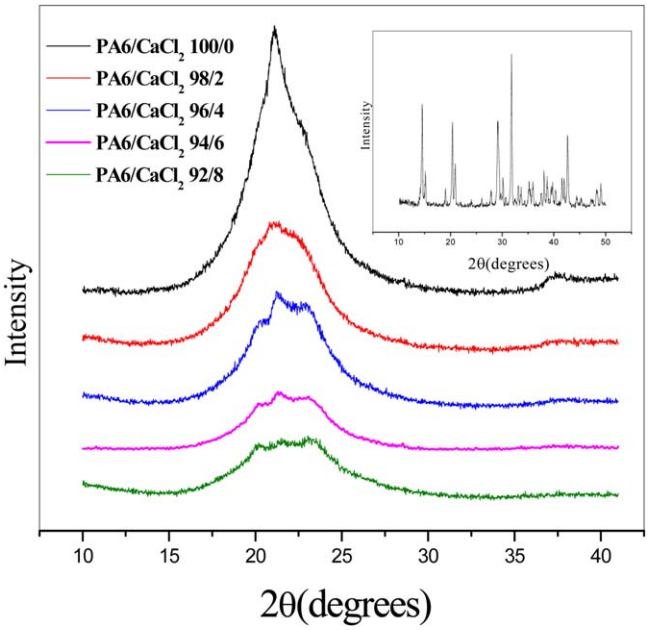

Figure 1. XRD of PA6 and PA6/$CaCl_2$ complex. [Color figure can be viewed in the online issue, which is available at wileyonlinelibrary.com.]

Mechanical Properties Tests. Tensile properties were performed using a material testing machine (WdW-10C, Shanghai Hualong Instrument Company, China) at a crosshead rate of 50 mm/min following the GB/T1040.2-2006 standard. Notched impact test was performed using an impact tester (XJUD-5.5, Xiamen Chongda Instrument Company, China) according to GB/T1043.1-2008 standard. The notched depth was 2 mm and the angular radius of the notch was 0.25 mm. All mechanical properties tests were performed at room temperature, and the values were calculated as averages from five samples at least.

RESULTS AND DISCUSSION

XRD Analysis

PA6 have polymorphism structures that mainly contain monoclinic γ-phase and α-phase.[16,17] In Figure 1, a diffraction peak of PA6 at $2\theta = 21°$ (001 and 200 planes) represents the γ-phase crystal, and the two medium diffraction peaks of PA6 at 20° (200 plane) and 24° (002 and 202 planes) are a distinctive feature of the α-phase crystal. XRD of $CaCl_2$ is shown in the inset in Figure 1. $CaCl_2$ has characteristic diffraction peaks at $2\theta = 14.5°$, 29.0°, and 31.5° that were not observed at all for the PA6/$CaCl_2$ complex, indicating that $CaCl_2$ completely reacts with PA6 during the melt compounding process.

To obtain the crystalline information of PA6 with different contents of $CaCl_2$, the crystallinity indices of the γ-phase and α-phase in PA6 and PA6/$CaCl_2$ complex were obtained by polynomial fitting.[18] During deconvolution analysis, the peak locations of γ-phase and α-phase were held constant, but the peak widths and heights were allowed to vary. For the amorphous phase, the peak location was allowed to float around 22°. To

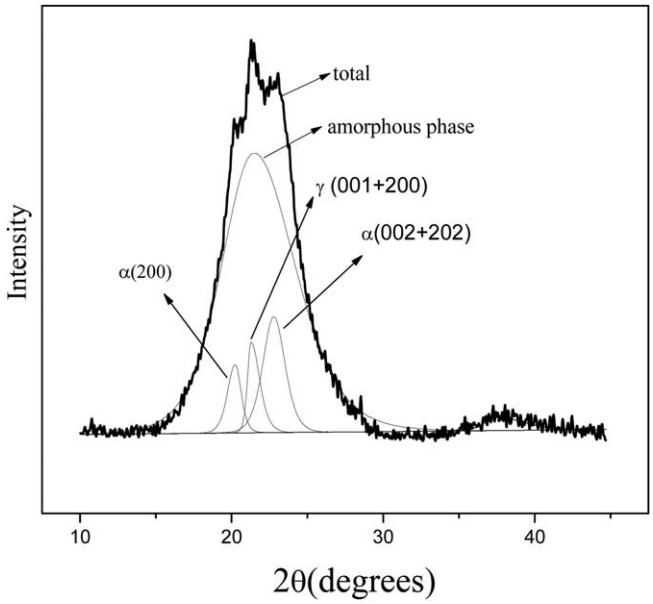

Figure 2. Deconvolution curves of PA6/$CaCl_2$ complex with 6 wt % $CaCl_2$.

start curve fitting algorithm reasonably, breadths and heights of each peak were adjusted manually, and they were modeled using a Gaussian–Lorentzian peak shape. Figure 2 showed an example of deconvoluted XRD peak of PA6/$CaCl_2$ complex with 6 wt % $CaCl_2$. To estimate the degrees of crystallinity for γ-phase and α-phase, the ratio of the areas of each phase to that of total area of the curve (crystalline + amorphous) was used. Besides, the model predictions and the data agreed well with determination coefficients R^2 being above 0.98. Results of these deconvolution analyses are shown in Table I. Because the complex reaction between $CaCl_2$ and PA6 destroyed intermolecular hydrogen bonds of PA6 and weakened the ability of molecular motion, total crystallinity (X_c) of γ-phase and α-phase reduced dramatically with increase of $CaCl_2$ contents. Besides, because the formation of γ-phase of PA6 was more difficult than the formation of α-phase, γ–α crystal transformation would occur, and the crystallinity ($X_{c\text{-}\gamma}$) of γ-phase decreased. In contrast, the crystallinity ($X_{c\text{-}\alpha}$) of α-phase initially increased and then decreased with the increase of $CaCl_2$ contents.

DSC Analysis

The cooling and heating curves of PA6 and PA6/$CaCl_2$ complex are shown in Figure 3 (a) and (b), respectively. The data are shown in Table II. Melting temperature (T_m) of PA6/$CaCl_2$ specimens reduced dramatically with the increase of $CaCl_2$ contents from 0 to 6 wt %. At $CaCl_2$ contents more than 6 wt %, the melting endotherms of PA6/$CaCl_2$ disappeared almost entirely. Moreover, as the contents of $CaCl_2$ increased from 0 to 4 wt %, double melting peaks appeared in the heating curves. At $CaCl_2$ contents equal to or more than 6 wt %, double melting peaks disappeared in the heating curves. Compared with XRD, the emergence of double melting peaks was mainly due to α-crystal in the high temperature and γ-crystal in the low temperature.[19] Small heat flux caused by γ-phase could not be detected by DSC at $CaCl_2$ contents equal to or more than 6 wt %, so the double melting peaks disappeared. What's more, the

Table I. XRD Results of PA6/$CaCl_2$ Specimens with Different Contents of $CaCl_2$

$CaCl_2$ content (wt %)	$X_{c\text{-}\gamma}$ (%)	$X_{c\text{-}\alpha}$ (%)	X_c (%)
0	29.8	4.6	34.4
2	7.9	16.8	24.7
4	4.8	17.9	22.7
6	2.7	16.9	19.6
8	1.1	7.9	9.0

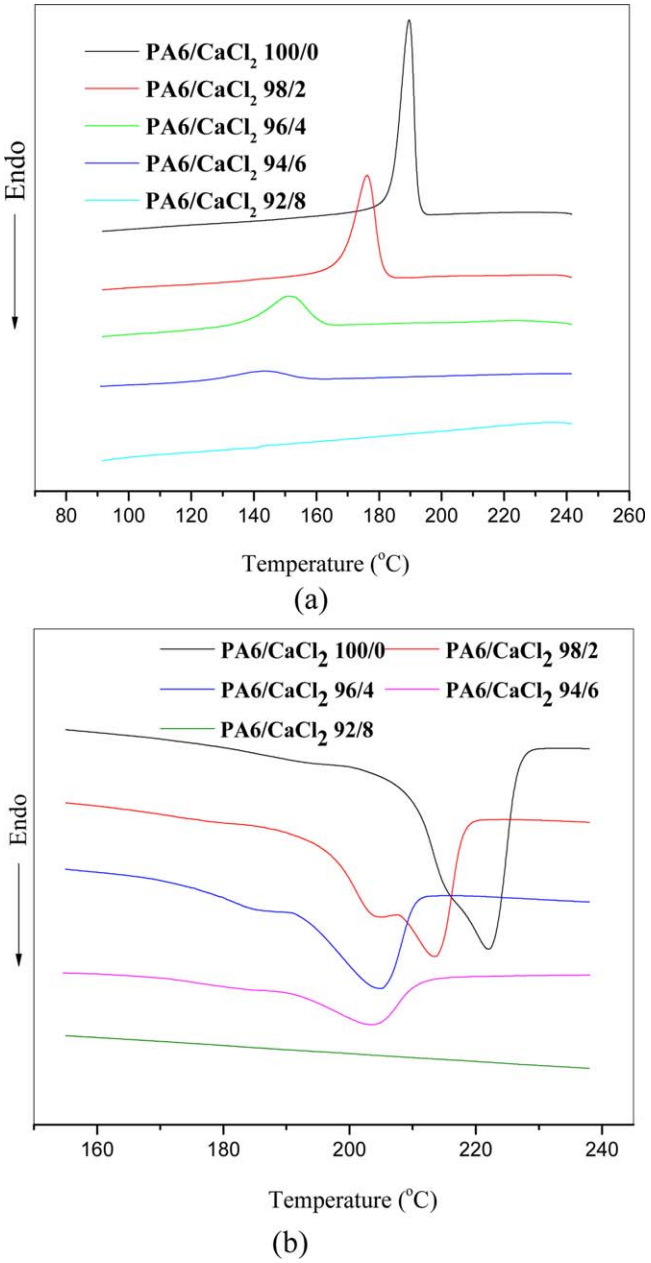

Figure 3. DSC cooling (a) and heating (b) curves of PA6/$CaCl_2$ specimens with different contents of $CaCl_2$. [Color figure can be viewed in the online issue, which is available at wileyonlinelibrary.com.]

Table II. DSC Results of PA6/$CaCl_2$ Specimens with Different Contents of $CaCl_2$

$CaCl_2$ content (wt %)	ΔH (J/g)	T_p (°C)	T_s (°C)	T_m (°C)	D (°C)	X_c (%)
0	89.06	189.61	192.34	222.08	5.47	37.11
2	79.04	176.18	181.01	213.44	8.78	33.61
4	42.05	150.62	161.70	204.51	10.60	18.25
6	16.77	143.06	158.32	203.41	18.52	7.43
8	-	-	-	-	-	-

X_c was determined by the following equation: $X_c = \frac{\Delta H_m}{\Delta H_0 \times \omega_{PA6}}$, where ΔH_0 represents heat of fusion of PA6, ΔH_m represents heat of fusion (240 J/g) of PA6 at 100% crystalline state, ω_{PA6} represents the mass fraction of PA6.

values of onset (T_s) and peak (T_p) of crystallization and X_c reduced consistently with the increase of $CaCl_2$ contents from 0 to 6 wt %. Compared with pure PA6, width at half height of crystallization (D) increased with the increase of $CaCl_2$ contents from 2 to 6 wt %.

The reduction of T_m was attributed to the imperfection of crystallization and decreasing of X_c. D represented the distribution of grain size and depended on the perfect degree of crystallization.[20,21] Increase of D indicated that imperfect degree of the crystal increased. Because of the amide groups in PA6 could complex with Ca^{2+}, the complexation between $CaCl_2$ and PA6 disrupted the intermolecular hydrogen bonds of PA6 and weakened the ability of molecular motion. So after blending $CaCl_2$ in PA6, imperfect degree of crystallization increased, and X_c reduced.

Dynamic Temperature Sweeps

Non-isothermal crystallization behaviors of PA6 and PA6/$CaCl_2$ complex by the rheological tests are shown in Figure 4. The shear modulus curves showed a slight increase (curve a-b), then a rapid increase (curve b-c), subsequently a gradual slow down increase (curve c-d) as temperature decreased. Following the work by Teh et al.,[22] at point "b," nucleation of PA6 commenced, which resulted in a rapid increase in modulus (curve b-c). At point "c," nucleation process was completed, and the increase in modulus (curve c-d) was due to crystal growth. In order to obtain accurately the crystalline information of PA6 with different contents of $CaCl_2$, the crystallization temperature in PA6 and PA6/$CaCl_2$ complex was obtained by derivative fitting. The data are shown in Table III. It can be seen that onset temperature (T_b) of nucleation and the growth temperature (T_c) of crystal reduced with the increase of $CaCl_2$ contents. Nucleation density measured by the increase in modulus at curve (b-c) also reduced with the increase of $CaCl_2$ contents. Besides, the rate of nucleation measured by the slope of curve (b-c) and the rate of crystal growth measured by the slope of curve (c-d) were also almost the same trend. The above results revealed that the presence of $CaCl_2$ had influenced crystallization of PA6. Because of the reduction of the rate of nucleation and the rate of crystal growth in the process of non-isothermal, imperfect degree of crystallization increased dramatically.

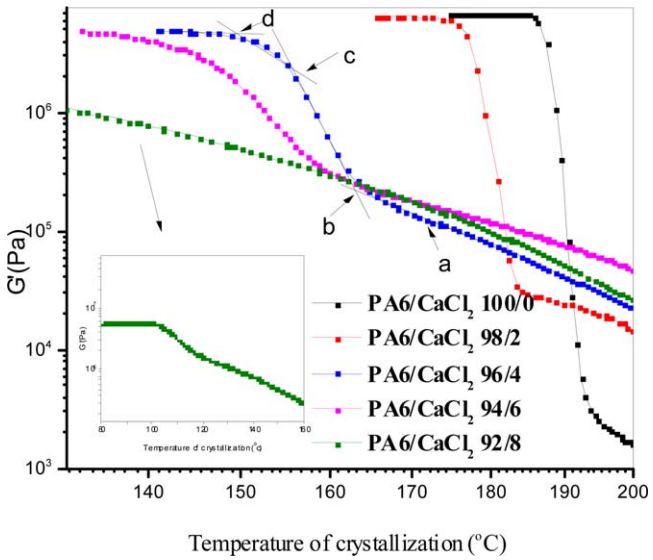

Figure 4. Dynamic mechanical tests on the crystallization behavior of PA6/$CaCl_2$ specimens with different contents of $CaCl_2$. [Color figure can be viewed in the online issue, which is available at wileyonlinelibrary.com.]

Compared the DSC with the rheology, the values of T_s and T_p by DSC were close to the values of T_b and T_c by rheological test with the increase of $CaCl_2$ contents from 0 to 6 wt %. This phenomenon revealed that although DSC and rheological test method were different, the results of crystallization behavior were almost equal. When the content of $CaCl_2$ was equal to 8 wt %, crystalline indices were not observed by DSC tests, which was attributed to small crystallization heat flux caused by confined crystallization of PA6. This phenomenon indicated that the rheological method for studying crystallization behavior of PA6/$CaCl_2$ complex was more sensitive than DSC. What's more, it was also capable of detecting transformation of the rate of nucleation and the rate of crystal growth.

Table III. Rheology Results of PA6/$CaCl_2$ Specimens with Different Contents of $CaCl_2$

$CaCl_2$ content (wt %)	T_b (°C)	T_c (°C)
0	192.50	189.65
2	181.05	175.88
4	162.04	150.11
6	158.78	143.67
8	123.93	113.72

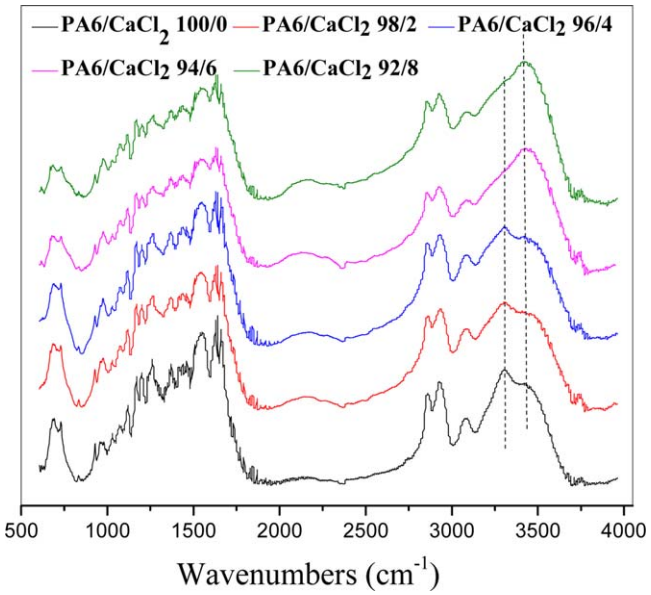

Figure 5. FTIR spectra of PA6/$CaCl_2$ specimens with different contents of $CaCl_2$. [Color figure can be viewed in the online issue, which is available at wileyonlinelibrary.com.]

FTIR Analysis

In order to reveal the mechanism of confined crystallization of PA6 with the increase of $CaCl_2$ contents, the FTIR of PA6 and PA6/$CaCl_2$ complex are shown in Figure 5. The bands for PA6 were documented in the literature.[23,24] Absorption bands were centered at 1529 (C—N stretching vibration of amide II band), 1640 (hydrogen-bonded C=O stretching vibration), 2900 (—CH_2— stretching vibration), 3300 (hydrogen-bonded N—H stretching vibration), and 3454 cm^{-1} (free state N—H stretching vibration). Besides, the bands at 1640 cm^{-1} and 3300 cm^{-1} strongly depended on intermolecular hydrogen bonds of PA6. After blending $CaCl_2$ in PA6, the strength of the peak at 3300 cm^{-1} weakened significantly, and the strength of the peak at 3400 cm^{-1} enhanced significantly. The reduction of intermolecular hydrogen bonds of PA6 indicated that crystallization of PA6 was confined after blending $CaCl_2$ in PA6, because hydrogen bonds of PA6 contributed to the ordered structure of the molecular chain and promoted crystallization of PA6.[25] What's more, because the amide group is a bi-functional electron donor with a sp^3 "lone pair" at the nitrogen atom and 2 sp^2 "lone pairs" at the oxygen atom, electron-donating sites to coordinate with Ca^{2+} have two possibilities. Overlap of 2 p_z orbitals of the oxygen, nitrogen atoms, carbon in the planar amide group would decrease the electron density of the nitrogen atom, and favor the coordination of Ca^{2+} with the carbonyl oxygen atom. So $CaCl_2$ is favorably of strong coordination with carbonyl and formation of PA6/$CaCl_2$ complex. Besides, the complexation interactions between Ca^{2+} and carbonyl are expected to confine the mobility of PA6 molecules in the process of crystallization, so crystallization of PA6 is confined.

Dynamic Frequency Sweeps

Storage modulus (G') and loss modulus (G'') versus frequency (ω) of PA6 and PA6/$CaCl_2$ complex are shown in Figure 6(a,b), respectively. As the contents of $CaCl_2$ increased, G'' of all the PA6/$CaCl_2$ specimens increased monotonously. From this result, it can be expected that the complexation interactions between Ca^{2+} and carbonyl made the friction force of segmental motion increase. At $CaCl_2$ contents less than 8 wt %, it was observed that G' of PA6/$CaCl_2$ specimens in Figure 6(a) turned up plateau at low frequency region.[26] What's more, plateau shifted to low frequencies gradually with the increase of $CaCl_2$ contents. The intermolecular hydrogen bonds of PA6 and the complexation interactions between $CaCl_2$ and PA6 caused the appearance of plateau at low frequency. After blending $CaCl_2$ in PA6, the complex reaction between $CaCl_2$ and PA6 disrupted the intermolecular hydrogen bonding and weakened the ability of molecular motion. Besides, the degree of complex reaction between $CaCl_2$ and PA6 increased, and the ability of molecular motion weakened with the increase of $CaCl_2$ contents.

Mechanical Properties

Tensile strength (σ_a) and notched Izod impact strength (σ_b) of PA6/$CaCl_2$ specimens are shown in Figure 7. As the contents of $CaCl_2$ increased, the σ_a and σ_b values of PA6/$CaCl_2$ specimens initially increased and then decreased. When the content of $CaCl_2$ was equal to 2 wt % and 6 wt %, the σ_a and σ_b values of

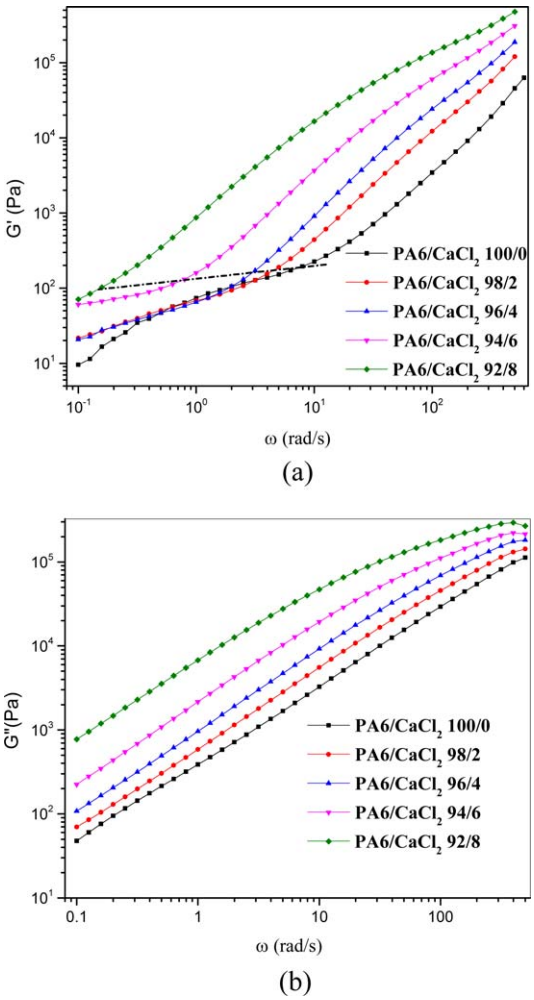

Figure 6. Storage modulus (G', a) and loss modulus (G'', b) versus frequency (ω) of PA6/$CaCl_2$ specimens at 230°C. [Color figure can be viewed in the online issue, which is available at wileyonlinelibrary.com.]

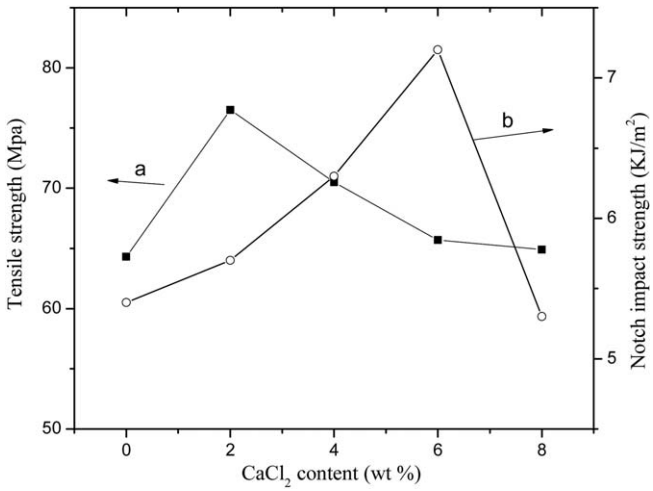

Figure 7. Mechanical properties of PA6/$CaCl_2$ specimens with different contents of $CaCl_2$.

PA6/$CaCl_2$ specimens reached optimum values, respectively. Compared with PA6, the σ_a and σ_b values of PA6/$CaCl_2$ increased by 19% and 33%, respectively. The mechanical properties were optimized at 2–6 wt % $CaCl_2$ where PA6 mainly formed α-phase crystal. It was possible that the α-phase crystal contributed to the improved mechanical properties. It can be seen that after blending $CaCl_2$ in PA6, the σ_a and σ_b values were almost higher than pure PA6. Although the complex reaction of Ca^{2+} with the carbonyl oxygen atom in the amide group made hydrogen bonding of PA6 disrupted and crystallinity of PA6 decreased, complexation interactions between $CaCl_2$ with PA6 were likely more stable than hydrogen bonds in PA6. Compared with pure PA6, the σ_a and σ_b values of PA6/$CaCl_2$ complex increased.

CONCLUSIONS

In this article, we presented a new approach to prepare low melting point PA6 by complex reaction of $CaCl_2$ and PA6 in a co-rotating twin screw extruder. Besides, we employed a new rheological method to study the crystallization behavior of PA6/$CaCl_2$ complex and the mechanism of confined crystallization of PA6. From the results of XRD, DSC, FTIR, rheology, and mechanical properties, as the contents of $CaCl_2$ increased, the total crystallinity of γ-phase and α-phase and crystallinity of γ-phase values of PA6/$CaCl_2$ specimens reduced dramatically, γ–α crystal transformation occurred, and the crystallinity of α-phase initially increased and then decreased. The rate of nucleation reduced significantly, and imperfect degree of crystallization increased dramatically. Moreover, tensile strength and notched Izod impact strength were improved after blending $CaCl_2$ in PA6. These were due to the complex reaction of $CaCl_2$ with the carbonyl oxygen atom in the amide group disrupted hydrogen bonding of PA6. Besides, the more stable complexation interactions between Ca^{2+} and carbonyl confined the mobility of PA6 molecules. This approach of preparing low melting point PA6 can broaden the insights for developing new PA6 with low melting points, and the rheological method explored in our study presents potential application in the detection of the crystallization behavior of other polymers.

ACKNOWLEDGMENTS

The authors gratefully acknowledge the financial support by Major Program of Science and Technology of Guizhou Province (No. 20136016), the National Natural Science Foundation of China (No. 50863001), and Special Foundation of Guizhou Province Outstanding Youth Science and Technology Talent (No. 201333).

REFERENCES

1. Sun, L.; Warren, G. L.; Davis, D.; Sue, H. J. *J. Mater. Sci.* **2011**, *46*, 207.
2. Peng, Y. X.; Chi, Y. L.; Dong, W. M.; Sun, D. M. *Mech. Compos. Mater.* **2013**, *49*, 245.
3. Li, J.; Zhang, J. *Polym. Plast. Technol.* **2011**, *50*, 969.
4. Unal, H.; Mimaroglu, A. *Int. J. Polym. Mater.* **2012**, *61*, 834.
5. Zhou, X.; Feng, J.; Cheng, D.; Yi, J.; Wang, J. *Polymer* **2013**, *54*, 4719.
6. Asundaria, S. T.; Patel, K. C. *Int. J. Polym. Mater.* **2010**, *59*, 370.
7. Ramiro, J.; Eguiazábal, J. I.; Nazábal, J. *Eur. Polym. J.* **2006**, *42*, 458.
8. Xiong, C. X.; Lu, S. J.; Wang, T.; Hong, Y.; Chen, T.; Zhou, Z. Y. *J. Appl. Polym. Sci.* **2005**, *97*, 850.
9. Afshari, M.; Gupta, A.; Jung, D.; Kotek, R.; Tonelli, A. E.; Vasanthan, N. *Polymer* **2008**, *49*, 1297.
10. Dong, L. J.; Xiong, C. X.; Wang, T.; Liu, D.; Lu, S. J.; Wang, Y. Z. *J. Appl. Polym. Sci.* **2004**, *94*, 432.
11. Wu, Y. J.; Xu, Y. Z.; Wang, D. J.; Zhao, Y.; Weng, S. F.; Xu, D. F.; Wu, J. G. *J. Appl. Polym. Sci.* **2004**, *91*, 2869.
12. Kotek, R. *Polym. Rev.* **2008**, *48*, 221.
13. Yu, J.; Hong, S.; Qian, Z. J.; Lu, S. J.; He, M. China Patent, CN10,1418,121 (**2009**).
14. Lu, S. J.; Zhou, Z. M.; Yu, J.; Li, F.; He, M. *Polym. Plast. Technol.* **2013**, *52*, 157.
15. Meng, L. M.; Huang, J. H.; Lin, Z. Y.; Qian, H. *Chem. Eng. Equip.* **2007**, *3*, 20.
16. Zhang, Y.; Hao, L.; Hu, G. *Polym. Plast. Technol.* **2012**, *51*, 780.
17. Shao, X. L.; Wei, Y. F.; Wu, L.; He, D. M.; Mo, H.; Zhou, N. L. *Polym. Plast. Technol.* **2012**, *51*, 590.
18. Ho, J. C.; Wei, K. H. *Macromolecules* **2000**, *33*, 5181.
19. Weng, W.; Chen, G.; Wu, D. *Polymer* **2003**, *44*, 8119.
20. Wang, B. B.; Wang, W.; Wang, H. P.; Hu, G. S. *J. Polym. Res.* **2010**, *17*, 429.
21. Ying, J. R.; Liu, S. P.; Guo, F.; Zhou, X. P.; Xie, X. L. *J. Therm. Anal. Calorim.* **2008**, *91*, 723.
22. Teh, J. W.; Blom, H. P.; Rudin, A. *Polymer* **1994**, *35*, 1680.
23. Vasanthan, N.; Salem, D. R. *J. Polym. Sci. Part B: Polym. Phys.* **2001**, *39*, 536.
24. Wu, Q.; Liu, X.; Berglund, L. *Polymer* **2002**, *43*, 2445.
25. Jia, J.; Raabe, D. *Eur. Polym. J.* **2006**, *42*, 1755.
26. Wu, G.; Zheng, Q.; Jiang, L.; Song, Y. H. *Chem. J. Chin. Univ.* **2004**, *25*, 357.